Migration Velocity Analysis using Time-Remigration Trajectory in Prestack Data

Tiago A. Coimbra, Henrique B. Santos*, Joerg Schleicher and Amélia Novais (UNICAMP & INCT-GP, Brazil)

This paper was prepared for presentation at the 13^{th} International Congress of the Brazilian Geophysical Society, held in Rio de Janeiro, Brazil, August 26-29, 2013.

Abstract

We present a prestack time-migration tool for improving the seismic velocity model in complex geological settings. The method is based on time-remigration trajectories. It determines kinematic parameters using local-slope information of seismic reflection events, which is extracted in an iterative process. These parameters, in turn, are used to correct the velocity model. The main advantage of this technique is that it allows to carry out a moveout correction not just at a fixed point in a zero-offset (post-stack) time-migrated gather, but varying through all offsets of a common image gather (CIG). In other words, it provides for migration velocity analysis (MVA) by time-remigration trajectories in prestack data. Tests on synthetic and SMAART-Sigsbee2B data show that the proposed tool not only increased the velocity-model resolution, but also provides a more plausible time-migrated image.

Introduction

Migration velocity analysis (MVA) is an important seismic processing step in prestack time-imaging. Basically, MVA exploits the redundancy of seismic data to improve an a-priori velocity model. As first observed by Sattlegger (1975), seismic data from different offsets need to migrate to the same positions when using the correct velocity model. Hence, these images are horizontally aligned, regardless of structure. However, too low or too high velocities lead to migration smiles or frowns (Al-Yahya, 1989; Zhu et al., 1998).

Over the past years, substantial effort has been directed towards proposing new MVA methods. Because of its conceptual clarity and simplicity, residual-moveout (RMO) analysis has become one of the favorite tools for MVA (Al-Yahya, 1989). However, in the case of strong dipping reflectors, this correction not takes into account the lateral displacement of reflectors caused by the change in migration velocity, thus requiring iterative procedures. Schleicher and Biloti (2007) tried to improved Al-Yahya's process and achieve higher accuracy in the updated velocity by inclusion of the reflector dip as an additional parameter.

Another process tries to follow reflection events through the migrated domain under variation of the migration velocity (Fomel, 1994; Liptow and Hubral, 1995). Hubral et al. (1996) used the term *image waves* to describe such a process of transforming time-migrated images according to the changes in migration velocity. Schleicher et al. (1997) derived equations for remigration trajectories in the zero-offset case and connected the concept to of residual migration. In a related way, Adler (2003) described the change in the superposition of seismic data along isochrons at a predicted image point as a function of the velocity perturbation, a process he called *Kirchhoff image propagation*. Fomel (2003a,b) further developed and tested the velocity-continuation or image-wave concept for the prestack situation.

Velocity continuation can be also used on migrated diffractions (Fomel et al., 2007; Novais et al., 2008) for MVA. Recently, Coimbra et al. (2013) demonstrated how to combine remigration trajectories with incorrectly migrated diffractions to update the velocity model. This technique makes use of local-slope information extracted from the data with the help of stacks along local trial surfaces. In this work, we present a method to construct a starting model for MVA using time-remigration trajectories for prestack data. Tests on synthetic and Sigsbee2B data, confirm the potential of our method to produce a plausible velocity model in a region with strong dip variation.

Theoretical Description

We are looking for the remigration trajectory, that is, an expression that describes the position in the prestack-migrated data volume at half-offset h of a horizontal reflector below a constant-velocity overburden with (true) average medium velocity v as variable of the function of vertical time τ, with the (incorrect) migration velocity v_m, initial vertical time τ_{h_0} and initial half-offset h_0 as parameters. We start from the expression of Al-Yahya (1989) in a single common-image gather, which yields the relationship between migrated times τ_{h_0} at h_0 and τ at h as

$$\tau_n(h) = \tau(h, v_n) = \sqrt{\tau_{h_0}^2 + 4\left(h^2 - h_0^2\right)\left(\frac{1}{v_n^2} - \frac{1}{v_m^2}\right)}. \qquad (1)$$

Additionally, based on the kinematics analysis of velocity continuation as presented by Fomel (2003b), we can approximate the remigration trajectory up to second order in h. This allows us to find the corresponding approximation of the two-way prestack residual migration path as

$$\tau_r(h,x) = \sqrt{\tau_n(h)^2 - \frac{4(x_r - x_m)^2}{v_m^2 - v^2} + 4h^2\left(\frac{1}{v_m^2} - \frac{1}{v^2}\right)}. \qquad (2)$$

The envelope of these curves defines the lateral displacement as

$$x_r = x(h) = x_m + \left(\frac{v_m^2 - v^2}{4}\right)\frac{\tau_{h_0}^2}{\tau_n(h)} D_{h_0}, \qquad (3)$$

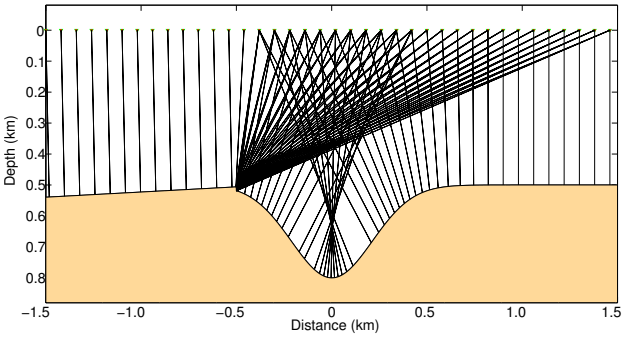

Figure 1: 2D sketch of a simple synthetic model and ray family. The model consist of two homogeneous halfspaces, separated by a reflector composed by a segment with small dip in the left portion, an edge diffractor caused by an abrupt change of direction, followed by a syncline and a horizontal reflector segment on the right side.

where the event dip can be written as

$$D(h) = D_{h_0}\frac{\tau_{h_0}}{\tau_n(h)}, \quad \text{where} \quad D_{h_0} = \frac{\partial \tau_{h_0}}{\partial x_m}. \tag{4}$$

For $h = 0$, equations (2) and (3) reduce to the zero-offset equations derived by Schleicher et al. (1997).

Combining equations (1)-(4) we arrive at the residual normal-moveout (RMO) expression

$$\tau_r(h) = \sqrt{\tau_n(h)^2\left(1 - \frac{v_m^2 - v^2}{4}D(h)^2\right) + 4h^2\left(\frac{1}{v_m^2} - \frac{1}{v^2}\right)}. \tag{5}$$

Since the residual moveout must be minimized at the correct velocity, we can choose the derivative of $\tau_r(h)$ as the objective function. Thus, the optimization condition is

$$\min_v \left\| \frac{\partial \tau_r}{\partial h} \right\|. \tag{6}$$

Here, we propose to use the above corrections in a sequential process. In this way, we are able to flatten a reflection event by an iterative estimation of a local slope through an image-wave propagation of the CIG.

To estimate the local slope $D(h)$, we define a surface $T = T(h,x)$ as

$$T(h,x) = \tau_n(h) + (x - x_m)D(h) = \tau_n(h) + (x - x_m)\frac{\tau_{h_0}}{\tau_n(h)}D_{h_0}. \tag{7}$$

This surface is tangent to traveltime surface (2), if the correct value of D_{h_0} is used. This fact can be used to estimate this parameter from the date by semblance maximization using trial surfaces.

Application to a simple synthetic test data set

We tested the technique of MVA using time-remigration trajectories as outlined above on a synthetic data set. The model (Figure 1) consists of a single trough-shaped reflector separating two homogeneous half-spaces with velocities 1.7 km/s and 1.9 km/s. Note that the reflector has a slight dip on the left side of the model and is horizontal on the right side. Moreover, there is an edge diffractor caused by an abrupt change of direction on the left shoulder of the syncline, indicated by the set of diffraction rays plotted in Figure 1.

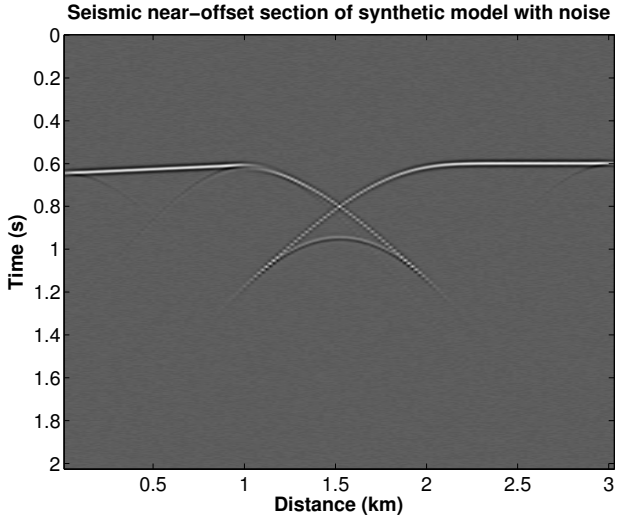

Figure 2: Noisy seismic near-offset section of the synthetic model presented in Figure 1. It was generated by Kirchhoff modeling with 151 traces at every 20 meters and a sampling rate of 4 ms and contaminated with white random noise at a level of 10% of the maximum amplitude.

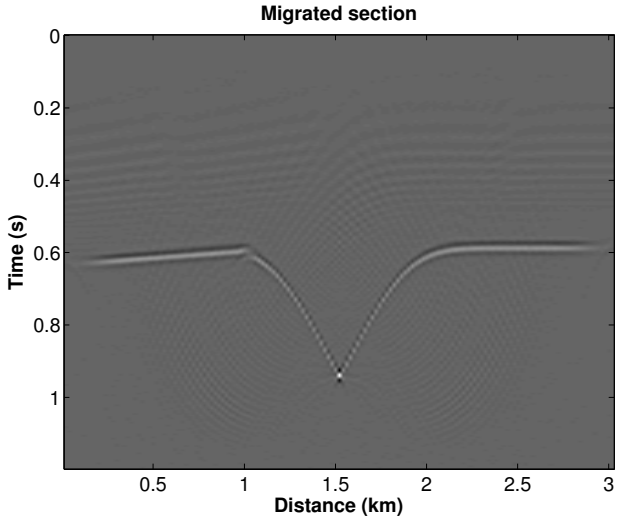

Figure 3: A single panel of a time migration of the seismic near-offset section (Figure 2) using a constant velocity $v_0 = 1.5$ km/s (water velocity) and migration aperture equal to 101 traces.

The synthetic data (Figure 2) were generated by Kirchhoff modeling with 151 traces at every 20 meters and a sampling rate of 4 ms and contaminated with white random noise at a level of 10% of the maximum amplitude. The trough-shaped reflector causes a caustic, evidenced by the distorted bow-tie structure in the data (Figure 2). The diffraction event has much smaller amplitude than the reflection event.

Supposing the true velocity of the upper layer unknown, we time-migrated these data with an arbitrarily chosen constant initial velocity. In this example, we chose the water

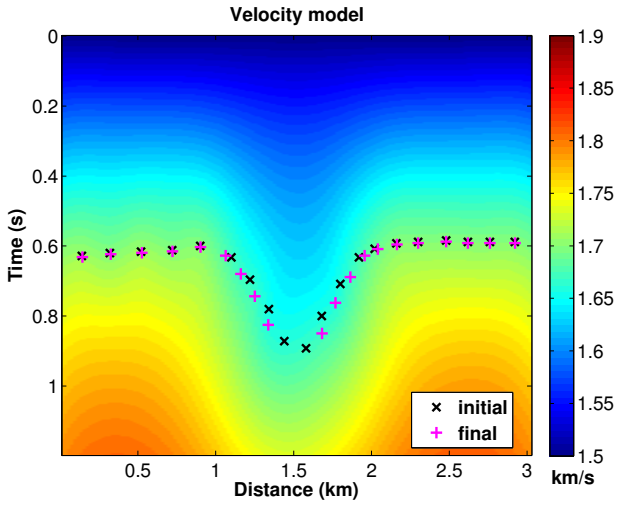

Figure 4: Updated velocity model using image point correction from constant velocity migration (one iteration). The black crosses represent the initial picked points in the migrated image (Figure 5), and the pink plusses indicate the corrected coordinates for the new velocity. This model was obtained by B-spline interpolation.

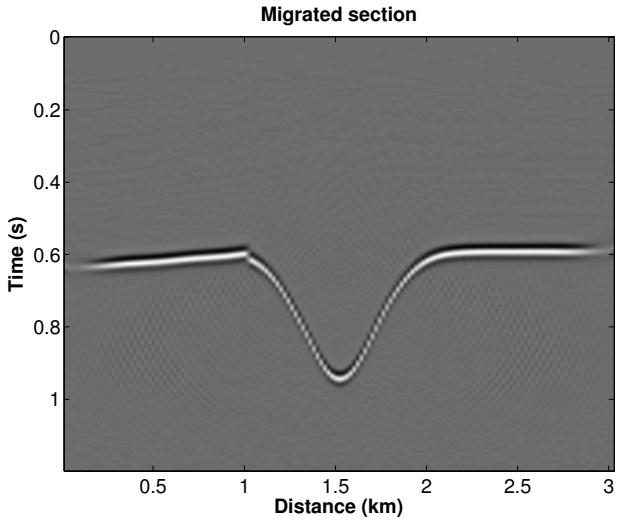

Figure 5: Final migrated image stack after velocity extraction using one iteration of image point correction. The migration aperture used was 101 traces.

velocity (for land-data, one might use some known near-surface velocity) $v_0 = 1.5$ km/s (Figure 3). We immediately recognize in this migrated image that the migration velocity was inadequately chosen, because the bow-tie structure from the synclinal reflector is not completely resolved. Also note that the edge diffractor is incorrectly imaged, with a spatial separation between the two reflector segments.

In this migrated section, we select specific points on reflection events (by manual clicks). The coordinates of each of these points define the present values of τ_{h_0} and x_m. In the CIG at x_m, we automatically determine the event slope D_{h_0} at h_0 as indicated in the context of equation (7). This slope value allows to apply an improved moveout correction to the chosen CIG according to equation (5). Moveout minimization according to equation (6) yields an improved velocity value and a corrected position for the chosen point in the image.

Figure 4 shows velocity model obtained after the first iteration of this procedure. The black crosses represent the initial picked points in the migrated image (Figure 3), and the pink plusses indicate their corrected coordinates in the improved velocity model. This model was obtained by B-spline interpolation of the information at the picked points. Note that the determined velocity in the region of the picks is closely approximating the true velocity of 1.7 km/s, with a maximum error of about 2%. Values outside the region of the picks are artifacts of the interpolation and carry no meaning.

Figure 5 depicts the final stack of all migrated images obtained from migrating all common-offset sections with the model of Figure 4. We see that the MVA by time-remigration trajectories nicely positions all parts of the reflector, confirming the good velocities in this region.

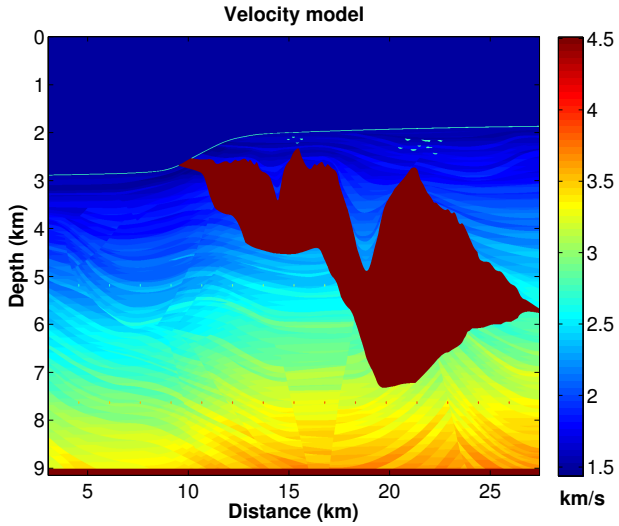

Figure 6: Complete Sigsbee2B stratigraphic velocity model.

Application to the Sigsbee2B data

For a more realistic test, we applied the described MVA technique to a subset of the Sigsbee2B NFS (no free surface) data set, so as to analyze complex structures like syncline segments over a salt structure. Figure 6 shows the Sigsbee stratigraphic velocity model.

The Sigsbee2B data contains traces at every 45.7 meters with a sampling rate of 8 ms. Figure 7 shows a short-offset section. The target area for our test is the region of the strong bow-tie structure from the syncline reflector at the salt top in the upper left part of the model (see box).

Since the Sigsbee2B data simulate a marine data set, we know the velocity of the first layer to be constant water velocity $v_0 = 1.5$ km/s. Thus, we choose this velocity for the first migration. Figure 8 depicts the migrated image of the target area obtained from the short-offset data of

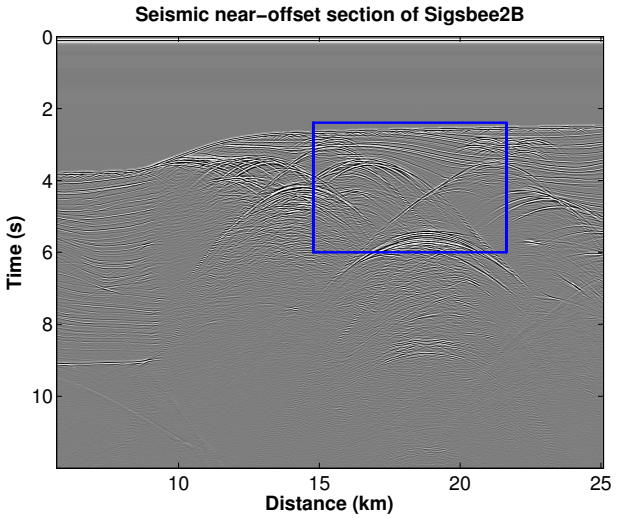

Figure 7: Seismic near-offset section of the complete Sigsbee2B data.

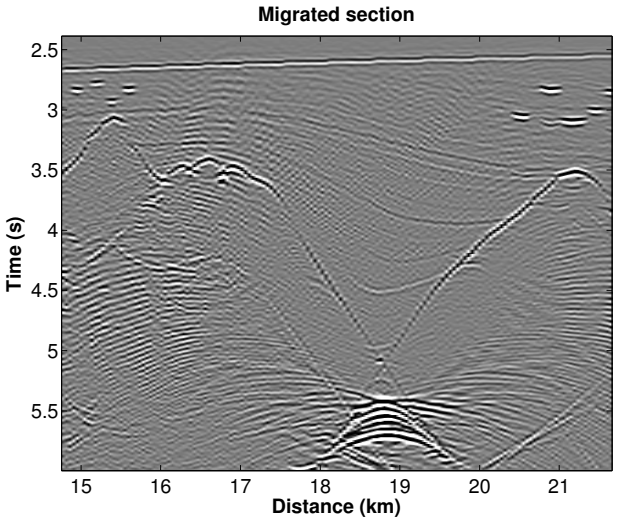

Figure 8: Time-migrated image of the seismic near-offset section using a constant velocity $v_0 = 1.5$ km/s (water velocity) and migration aperture equal to 141 traces.

Figure 7. The migration aperture used was 141 traces. As expected, this first migration is not able to resolve the bow-tie structure or focus the reflection energy.

Next, to apply the MVA by time-remigration trajectory as discussed above, we picked several points on some of the most prominent migrated events in the image of Figure 8. The coordinates of these picks define CIGs where we extract local slopes and minimize residual moveouts. Figure 9 shows the picks (black crosses) and their corrected positions after velocity updating (pink plusses) overlain on the resulting velocity model. It is easy to see that the coordinates are corrected more strongly in the syncline region, where the initial velocity is further from the true velocity, than in the upper part of the model, where the water velocity is much closer to the true medium velocity.

We then used the velocity model of Figure 9 for a new

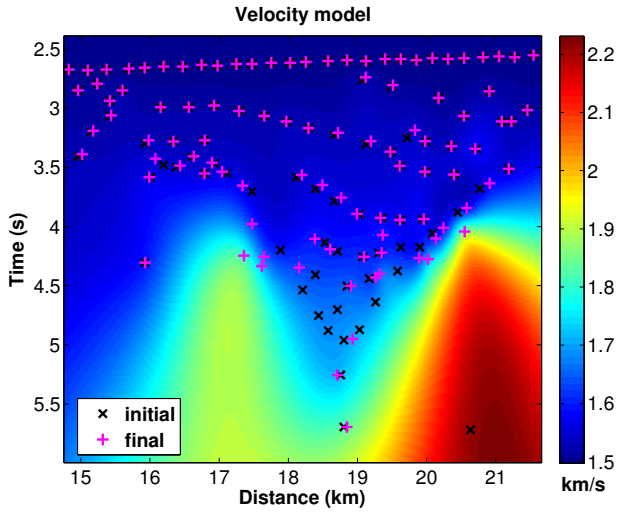

Figure 9: Velocity model extracted using image point correction from constant velocity migration (first iteration). The black crosses represent the initial picked points in the migrated image of Figure 8, and the pink plusses indicate the corrected coordinates for the updated velocity. The overall model was obtained by B-spline interpolation.

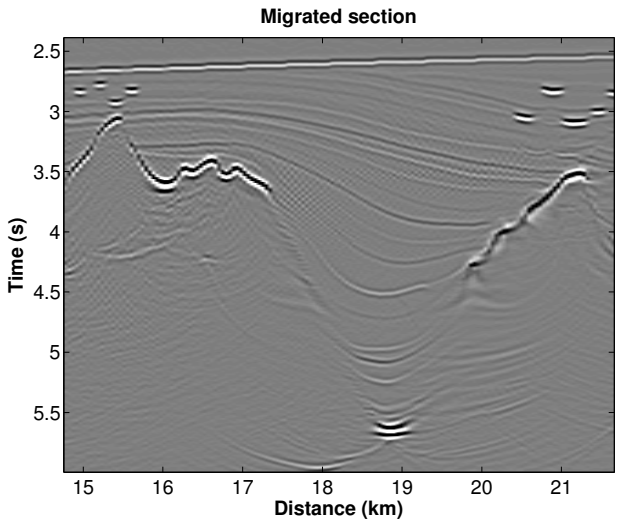

Figure 10: Migrated image after velocity extraction using one iteration of image point correction. The migration aperture used was 141 traces.

migration of the target region. The result is depicted in Figure 10. We immediately recognize that the shallower parts of the salt top have been nicely improved in this image, indicating that the velocity model in this region already has reached acceptable quality. Certainly, the same cannot be said of the salt flanks. Therefore, we have repeated the procedure of reflector picking and velocity updating for a second set of points picked in this new migrated image.

Figure 11 shows the velocity model after this second iteration together with the picked points (black crosses) and their updated positions (pink plusses). We note that the displacements are smaller than in Figure 9, indicating convergence of the method.

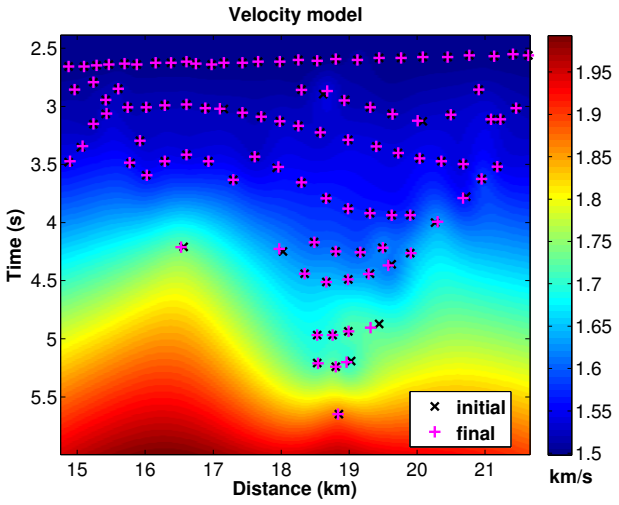

Figure 11: Velocity model after second iteration. The black crosses represent the initial picked points over the migrated image (Figure 10), and the pink plusses indicate the corrected coordinates of the newest velocity. The complete model was obtained by B-spline interpolation.

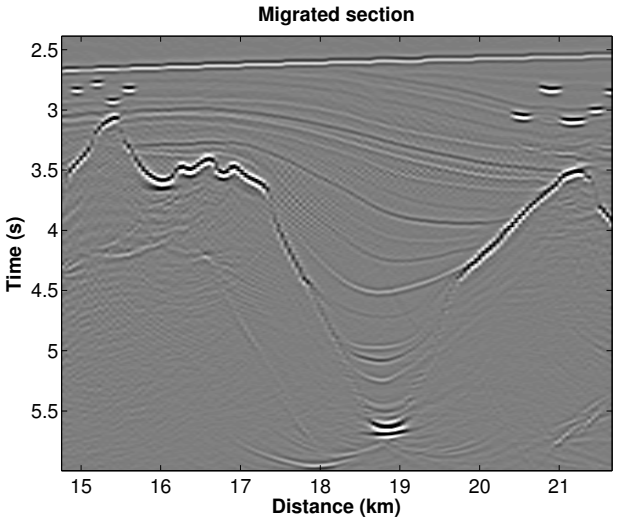

Figure 12: Final migrated image stack after two iterations of velocity extraction using remigration trajectories. The migration aperture was 241 traces.

The corresponding migrated image is depicted in Figure 12. For this migration, we used a migration aperture of 241 traces. In comparison to Figure 10, the flanks of the synclinal structure are much better focused and the bottom of the trough is correctly positioned.

To evaluate the quality of the final velocity model, let us look at three selected CIGs at positions 16.56, 18.85 and 20.54 km (Figures 13, 14 and 15, respectively). On the whole, it is easy to observe that the strongest events, mainly the shallow ones, were completely flattened. The first CIG at 16.56 km (Figure 13) allow us to analyze the edge diffraction at the salt bottom at about 4.2 s (see also the model in Figure 6). It shows that our method flattened the diffraction event. The second CIG at 18.85 km (Figure 14) represents the central part of the Sigsbee2B

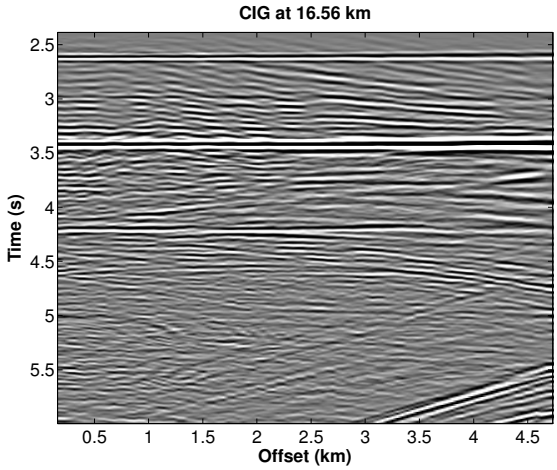

Figure 13: Common-image gather at 16.56 km.

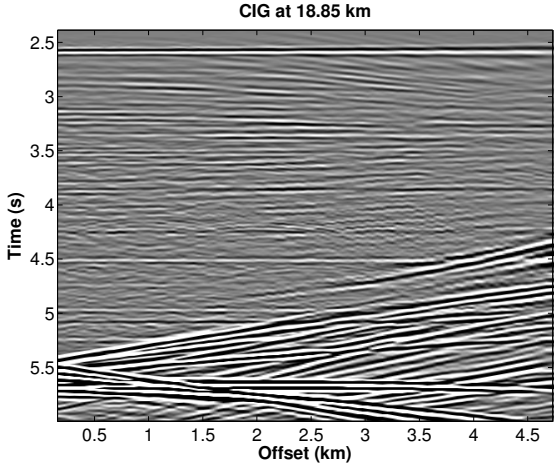

Figure 14: Common-image gather at 18.85 km.

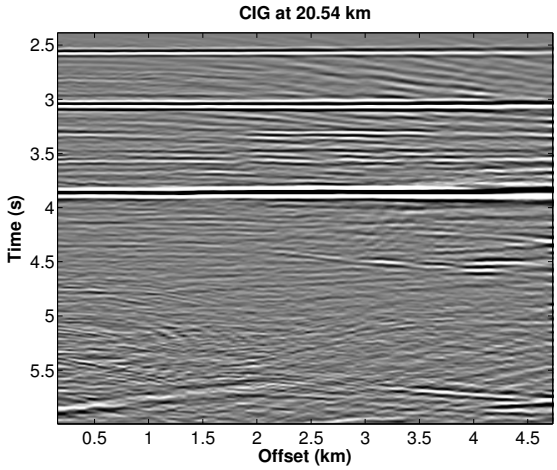

Figure 15: Common-image gather at 20.54 km.

syncline. Here, we call attention to the high amplitudes below 5 seconds due to multiple reflections in this syncline. Nevertheless, it is possible to observe the nearly flattened event of the bottom of the trough at about 5.6 seconds. The third CIG at 20.54 km (Figure 15) shows the right portion of the syncline, where the salt structure is thicker and where shallow diffractors are present. We note that down to the salt top, all events are nicely flattened. The deeper events

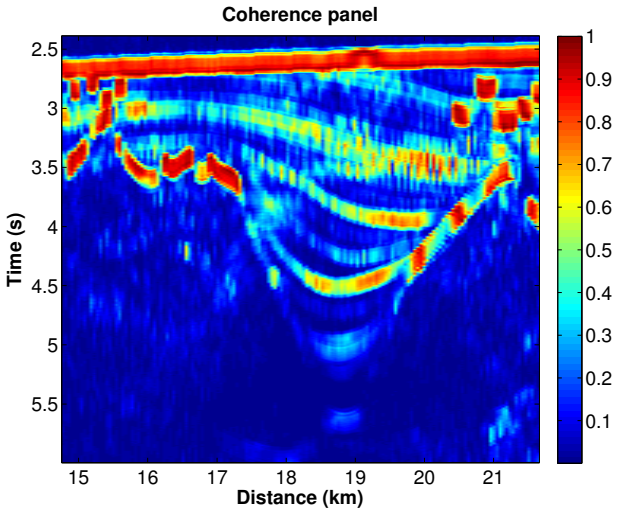

Figure 16: Coherence panel after the second iteration.

were not included in the present analysis.

Finally, in Figure 16 we present the coherence painel corresponding to the second migration, i.e., the semblance in the corresponding CIG at each point of the migrated image of Figure 12. All main events down to the top salt are well imaged, and even the edge diffractor at the salt bottom is clearly visible. The slight residual moveout of the bottom-of-the-trough reflection in the CIG of Figure 15 results in its poor visibility in this panel.

From the analysis of the coherence panel, the CIGs and the final migrated image, we conclude that MVA using time-remigration trajectories constitutes a powerful tool to improve the positioning of key reflectors in a migrated image and update the velocity model correspondingly, at least in sedimentary regions. The focused edge diffraction event at the salt bottom gives rise to hopes that the method will also work in more complex areas. The computational cost of the technique is determined by the cost of prestack time migration in each iteration. Intermediate computations are negligible.

When testing our method, we noted that the resulting velocity models were strongly dependent on the method chosen to interpolate the velocity between the positions of the picks. However, the resulting images were rather similar to each other, providing another confirmation for the robustness of time migration with respect to velocity errors. For the presentation in this work, we chose the models obtained by B-splines interpolation of Matlab (Sandwell, 1987).

Conclusions

We have developed a tool that uses the estimation of local kinematic attributes of selected events in seismic data to update the velocity model and improve the positioning of key reflectors. The method is based on image-wave propagation in the CIG domain described by the means of time-remigration trajectories in the prestack time-migrated domain. Such a trajectory is defined as the set of points where a certain point on a reflection event is migrated to as a function of migration velocity.

The methods consists of analyzing the local slope of selected key reflections and determining the velocity value for which an approximate residual-moveout expression is minimized. The advantage of this procedure over conventional MVA methods is that the RMO expression follows the events outside a fixed CIG. In our numerical tests, this led to acceptable velocity models in very few iterations, even if the starting model was simply constant water velocity. The sedimentary shallow part of the Sigsbee2B model was satisfactorily resolved in two iterations. The computational cost of the technique is determined by the cost of prestack time migration in each iteration. Intermediate computations are negligible.

Acknowledgments

This research was supported by Petrobras and CGG as well as the Brazilian national research agencies CNPq, FAPESP, and CAPES. The second author (HBS) thanks CGGVeritas-Brazil for his fellowship. Additional support for the authors was provided by the sponsors of the *Wave Inversion Technology (WIT) Consortium*. We would like to thank the SMAART JV for providing the Sigsbee2B NFS dataset.

References

Adler, F., 2003, Kirchhoff image propagation: Geophysics, **67**, 126–134.

Al-Yahya, K. M., 1989, Velocity analysis by iterative profile migration: Geophysics, **54**, 718–729.

Coimbra, T. A., J. J. S. de Figueiredo, J. Schleicher, A. Novais, and J. Costa, 2013, Migration velocity analysis using residual diffraction moveout in the poststack depth domain: Geophysics, **78**, S125–S135.

Fomel, S., 1994, Method of velocity continuation in the problem of seismic time migration: Russian Geology and Geophysics, **35**, no. 5, 100–111.

———, 2003a, Time migration velocity analysis by velocity continuation: Geophysics, **68**, 1662–1672.

———, 2003b, Velocity continuation and the anatomy of residual prestack time migration: Geophysics, **67**, 1650–1661.

Fomel, S., E. Landa, and M. T. Taner, 2007, Poststack velocity analysis by separation and imaging of seismic diffractions: Geophysics, **72**, U89–U94.

Hubral, P., M. Tygel, and J. Schleicher, 1996, Seismic image waves: Geophysical Journal International, **125**, 431–442.

Liptow, F., and P. Hubral, 1995, Migrating around in circles: The Leading Edge, **14**, 1125–1127.

Novais, A., J. Costa, and J. Schleicher, 2008, GPR velocity determination by image-wave remigration: Journal of Applied Geophysics, **65**, 65–72.

Sandwell, D. T., 1987, Biharmonic spline interpolation of GEOS-3 and SEASAT altimeter data: Geophysical Research Letters, **2**, 139–142.

Sattlegger, J. W., 1975, Migration velocity determination: Part I. philosophy: Geophysics, **40**, 1–5.

Schleicher, J., and R. Biloti, 2007, Dip correction for coherence-based time migration velocity analysis: Geophysics, **72**, S431–S48.

Schleicher, J., P. Hubral, and G. Höcht, 1997, Seismic constant-velocity remigration: Geophysics, **62**, 589–597.

Zhu, J., L. Lines, and S. Gray, 1998, Smiles and frowns in migration/velocity analysis: Geophysics, **63**, 1200–1209.